Far Infrared Spectroscopy of the HH 1/2 Outflow[1]

Sergio Molinari

Istituto di Fisica dello Spazio Interplanetario - CNR, Via Fosso del Cavaliere, I-00133 Roma, Italy

Alberto Noriega-Crespo

SIRTF Science Center & Infrared Processing and Analysis Center, California Institute of Technology, MS 100-22, Pasadena, CA 91125

Received _____; accepted _____

ABSTRACT

The HH 1/2 system has been observed with the two spectrometers on board the Infrared Space Observatory. Diffuse [CII]158μm emission indicate the presence of a Photo-Dissociation Region (PDR) which is only in part due to the external Far-UV irradiation from the nearby Orion Nebula. Additional irradiation must be originated locally and we show that the FUV field produced in the recombination regions behind the shocks traced by the HH objects is sufficient to induce a PDR at the flow cavity walls.

The analysis of [OI], [SiII]34.8μm and [NeII]12.8μm lines suggests shock velocities $v_s \sim 100 \div 140$ km s^{-1} with pre-shock densities between 100 and 1000 cm^{-3}. H_2 pure rotational lines trace a T$\sim$600 K gas which is likely to be warmed up in slow, planar, molecular shocks. The coexistence in the areas subtended by the instrumental beamsizes of shocks at different velocities is consistent with the bow-shock morphology of the HH 1 and, to a lesser extent, HH 2 as traced by optical images.

Subject headings: Stars: formation - (ISM:) Herbig-Haro objects - ISM: individual objects: HH 1/2 - ISM: molecules - Infrared: ISM: lines and bands

---

[1]ISO is an ESA project with the instruments funded by ESA Members States (especially the PI countries: France, Germany, the Netherlands and the United Kingdom) and with the participation of ISAS and NASA.

1. Introduction

The HH 1/2 is still the proto-typical optical Herbig-Haro (HH) outflow, and has been and it is the subject of large number of studies at almost all possible wavelengths, sensitivities and angular resolutions (see "Notes" in Reipurth Reipurth (1999) for nearly 100 references on this young stellar bipolar flow). Some of the most recent studies, however, have concentrated on the molecular gas properties and its relationship to the optical emission, particularly in the context of entrainment, shock chemistry, proper motions, multiple outflows, multiple ejection events and the 'unified model' for stellar jets-CO flows. It is in this realm that studies of the far-infrared emission are of great importance, since in these collisionally excited objects a large fraction of the atomic and molecular gas cooling takes place at these wavelengths (see e. g. Saraceno 1998; Molinari et al. 2000).

A quick reminder of the HH 1/2 bipolar jet properties goes as follows; it lies in Orion at ~ 460 pc, with an angular size of $\sim 3'$ on its brightest component but with signatures of shock excited emission from a previous ejection event $\sim 23'$ NW from VLA 1, the outflow's embedded Class 0 driving source (Ogura 1995; Pravdo et al. 1985). The proper motions indicate flow velocities of $\sim 300 - 400$ km s^{-1} for both the atomic/ionic and warm H_2 gas (Herbig & Jones 1981; Eislöffel, Mundt & Böhm 1994; Rodriguez et al. 2000; Noriega-Crespo et al. 1997), and this sets a dynamical age of $\sim 6 \times 10^5$ yrs for the outflow, but with a major ejection event some $\sim 7.5 \times 10^4$ yrs ago, defined by the brightest condensations. Recent single-dish radio observations have shown that the J=1-0 CO emission is bounded by the ionic/atomic gas (Moro-Martin et al. 1999), thus providing strong support to the idea that molecular outflows are driven by the stellar jets themselves (see e.g. Raga 1994).

The Infrared Space Observatory (ISO, Kessler et al. 1996) observed HH 1/2 with the mid-IR camera (CAM) and the short and long spectrometers (SWS & LWS respectively). A partial analysis of circular variable filter (CVF) ISOCAM observations showed the presence

of strong ground rotational H_2 emission lines with a morphology quite similar to that of the NIR H_2 gas. These data also showed some signatures of strong J-shocks, like [NeII]12.8μm, as expected in high excitation HH outflows (Cernicharo et al. 1999). In this study we present the analysis of the ISO SWS and LWS data with an emphasis on the properties of shocks in the HH 1/2 outflow and their effects on the immediately surrounding medium. A summary of the observations and data reduction techniques is presented in §2, followed by a presentation of the results (§ 3) and their discussion (§ 4).

2. Observations and Data Reduction

The Long Wavelength Spectrometer (LWS, Clegg et al. 1996) was used in its LWS01 grating mode to acquire full low resolution (R $\sim$ 200) 43-197μm scans with data collected every 1/4 of a resolution element (equivalent to $\sim$0.07μm for $\lambda \lesssim 90\mu$m, and to $\sim$0.15μm for $\lambda \gtrsim 90\mu$m); a total of 25 scans were collected, corresponding to 50s integration time per spectral element.

LWS data processed through Off-Line Processing (OLP) version 7, have been reduced using LIA, the LWS Interactive Analysis[2] Version 7.3. The package consists in a set of tools to inspect in great detail the data quality at the photocurrent level. We have refined the dark currents and gain for each detector; temporal trends in these two parameters were also estimated and subtracted/divided. Finally, the data were recalibrated in wavelength, bandpass and flux. The absolute flux calibration accuracy for LWS in grating mode is 10% (ISO Handbook, IV, 4.3.2).

The Short Wavelength Spectrometer (SWS, de Graauw et al. 1996) was used in the SWS02 grating line profile observing mode, covering 8 lines: Brγ, H2 S(1) - S(5),

[2]LIA is available at http://www.ipac.caltech.edu/iso/lws/lia/lia.html

[NeII]12.8μm and [SiII]34.8μm, achieving a spectral resolution R$\sim 900 - 2000$ (see Table 2.2 ISO Handbook 1.1, p 9). The SWS data was processed using OSIA[3], the SWS Interactive Analysis software, that permits to revise the performance of the dark current and photometric checks calibration. As in previous work we have used the latest (November 2000) bandpass calibration files to produce the final spectra.

The final steps of data analysis were done for both LWS and SWS data using ISAP, the ISO Spectral Analysis Package Version 2.0[4]. Grating scans (for LWS) and detectors spectra (for SWS) were averaged using a median clipping algorithm optimized to flag and discard outliers mainly due to transients. Significant memory effects were present in LWS detectors LW2, 3 and 4, in the form of systematic differences between the two grating scan directions. The LWS observations toward all positions were heavily fringed, partly due to the presence in the area of the so-called Cohen-Schwartz (C-S) star (Cohen & Schwartz 1979), partly for likely extension of the detected FIR emission; standard techniques available under ISAP were used to remove these instrumental effects.

3. Results

The region observed with the ISO spectrometers is pictured in Fig. 1, where the relevant objects are identified and the locations of the LWS and SWS beams are also indicated. The C-S star is a $\sim$30 $L_\odot$ T Tauri star (Cohen et al. 1984) that was believed to be the exciting source of the bipolar flow before VLA 1 was discovered by Pravdo et al. (1985).

[3]OSIA is available at http://sws.ster.kuleuven.ac.be/osia

[4]ISAP is available at http://www.ipac.caltech.edu/iso/isap/isap.html

EDITOR: PLACE FIGURE 1 HERE.

Line detection was established by visual inspection of the averaged spectra, and Gaussian functions were fitted to estimate integrated line fluxes. In order for a line to be considered as detected, it had to be consistently present in both scan directions. This is particularly critical for lines in the LWS spectral range between ∼110 and 160μm, where detector memory effects were clearly identified (§2). Figure 2 show the lines detected with the two spectrometers.

EDITOR: PLACE FIGURE 2 HERE.

To estimate uncertainties we multiplied the standard deviation of the fit from the data by the width of the spectral resolution element. Computed values are reported in Table 1. Line and continuum flux was observed from all LWS pointed positions. The LWS beam has a nearly Gaussian shape, so that radiation may be collected from outside the nominal FWHM beamsize. At the distance of one beam this contamination will be of the order of 10-20%, and since the observed positions with the LWS are adjacent, we can in principle estimate the true flux coming from within the individual beams. In the case of the HH 1 and HH 2 pointings, contamination is only due to the flux coming from VLA 1 (the two HH objects are too far to reciprocally contaminate each other). Instead, the observed flux from VLA 1 will be contaminated from both HH 1 and HH 2. The contamination corrected flux for the lines detected with the LWS are reported in italic in Table 1

EDITOR: PLACE TABLE 1 HERE.

Giannini, Nisini & Lorenzetti (2001) have recently independently reduced the same ISO-LWS data toward HH 1/2. Compared to theirs, our reduction includes the full data

reprocessing through the LWS Interactive Analysis (§ 2) which is crucial to really have a handle on the level of reliability of the calibrated data. By averaging scan directions separately we were able to estimate the line fluxes using the more reliable scan direction when detector memory effects were identified (§2). Maybe as a result of this higher level of analysis, we have not reported as detected in Table 1 a number of lines (mainly CO lines) which are instead reported as detected by Giannini, Nisini & Lorenzetti (2001). However, for the lines commonly reported as detected the fluxes are in substantial agreement (within 10%) for the brighter lines; for fainter lines the discrepancy can be as high as a factor two, but the relative uncertainties in the flux estimates are also as large.

Few basic considerations will help set the frame for the subsequent discussion. [CII]158μm is detected toward all LWS pointings. Since [CII]158μm line is one of the main coolants in FarUV-irradiated gas, it seems natural to postulate its origin in a Photo-Dissociation Region (PDR, see e.g. Tielens & Hollenbach 1985). Post-shock cooling regions may also produce [CII]158μm, but this is not relevant in the present case because the implied levels of [OI]63μm, expected to be at least ten times stronger than [CII]158μm for a wide range of shock velocities and pre-shock densities (e.g., Hollenbach & McKee 1989), are simply not observed. The origin of [OI] lines, also detected toward all observed positions, is more difficult to assess; [OI]63μm, definitely the main shock coolant, can be an important (and even dominant) cooling line in PDRs too, if the density is n$\gtrsim 10^4$ cm^{-3} and the FUV irradiation level, expressed in units of 1.6 10^{-3}ergs s^{-1} cm^{-2}, the local interstellar radiation field (Habing 1968), is $G_0 \gtrsim 10^2$ (Kaufman et al. 1999). There is very little doubt, however, that a major contribution to [OI] emission comes from shocks since [SiII]34.8μm and [NeII]12.8μm, both important coolants in dissociative shocks, are also detected in the present observations; a conclusion further supported by the theoretical J-shock modeling (Hartigan, Raymond & Hartmann 1987; Hartigan, Morse & Raymond 1994) applied to the strong optical [OI] 6300+6363 Å emission along the entire outflow (Solf & Böhm

1991). So to explain the observed FIR line emission we need to invoke at least two physical mechanisms; a PDR for[CII]158μm and shocks for at least part of [OI]. A detailed analysis of the physical conditions of the PDRs in which the [CII]158μm line is generated will provide an estimate of the relative fractions of [OI] lines radiated by the two mechanisms.

4. Discussion

4.1. The PDR

[CII]158μm line has similar fluxes, within 20%, along the flow; in particular, the line is stronger toward HH 2 and fainter toward VLA 1. On this basis, we exclude both the C-S star and the heavily embedded VLA 1 source as the FUV (between 6eV and 13.6eV) field sources responsible for the PDR conditions. Either the FUV field source is external to the HH 1/2 flow, or, if local, must be somehow distributed along the flow. We will see below that a combination of the two possibilities best explains the observations.

4.1.1. External irradiation

The external irradiation hypothesis is supported by the evidence (Mundt & Witt 1983) of a significant UV irradiation on the HH 1/2 area from the Orion nebula, whose center lies $\sim 1.5^\circ$ to the north. This contamination would amount to 30$\div$50% of the flux levels detected toward HH 1/2 shortward of $\sim$1500Å, decreasing to $\sim$20% at longer wavelengths. Based on the IUE measured spectra (Böhm-Vitense et al. 1982; Böhm, Noriega-Crespo & Solf 1993) the integrated FUV field due to irradiation from the Orion Nebula would amount to $G_0 \sim 7$, although it should be noted that the data used by Mundt & Witt (1983) do not go shortward of $\sim$ 1500Å. This value is compatible with the FUV field from the dominant Trapezium star θ_c^1 (about $G_0 \sim 18$), with a reasonable amount of extinction along the path

to HH 1/2. The maximum [CII]158μm line flux in the ISO-LWS beam (assuming complete beam filling) that can be produced by this FUV field is $\sim 3.5\ 10^{-19}$ W cm^{-2} for a gas density n$\sim 10^3$ cm^{-3} (Kaufman et al. 1999). The [CII]158μm flux decreases by about 40% for densities a factor 10 higher or smaller, and is almost linear with G_0. We conclude that about half, at most, of the PDR [CII]158μm emission measured by ISO-LWS may be due to external irradiation by the Orion Nebula.

4.1.2. Local irradiation

In a recent paper (Molinari, Noriega-Crespo & Spinoglio 2001) we proposed that the [CII]158μm flux detected toward the HH objects in the HH 80/81 flow was emitted in a PDR situated at the walls of the cavity excavated by the flow, and irradiated by collisionally-enhanced 2-photon FUV continuum emitted by the post-shock ionized regions in the HH objects (Dopita, Binette & Schwartz 1982). We propose that this scenario is also pertinent to the HH 1/2 system. In terms of observables, this model establishes a relationship between the free-free radio continuum emitted by the recombination region in the HH object, and the [CII]158μm line flux radiated by the PDR at the cavity walls. In the optically thin regime, the former can be expressed as (Curiel, Cantó and Rodríguez 1987):

$$S_\nu = 1.84 \cdot 10^{-4}\ \theta^2\ \left[\frac{\nu}{10\ GHz}\right]^{-0.1}\ T_4^{0.45}\ n_{o_{10}}\ v_{s_7}\ [1 + 3.483 v_{s_7} - 2.745]\ \mathrm{mJy} \qquad (1)$$

θ is the angular diameter of the recombination region and is estimated off-the-plot from the 6 cm VLA D-conf. maps of Rodríguez et al. (1990) to be $\sim 10''$. T_4 is the electrons temperature in units of 10^4 K and we hold it fixed at 1 in these units. v_{s_7} is the shock velocity in units of 100 km s^{-1} and we fix it to 1 in these units as determined in § 4.2.1 below. $n_{o_{10}}$ is the pre-shock density in units of 10 cm^{-3} and we will keep this as the only

free parameter in Eq.(1).

The [CII]158μm line flux can be expressed as (Molinari, Noriega-Crespo & Spinoglio 2001):

$$F_{Cii} = \frac{10^{-7}}{D^2}\frac{4\pi}{3} r_{HH}^3 \; \eta_{ce} \; f_c \; \chi_c \int_{6eV}^{13.6eV} j_\nu d\nu \; \mathrm{W\,cm^{-2}} \qquad (2)$$

D is the distance of the source from the Sun. j_ν is the 2-photon process emissivity and is a function, among other things, of the square of gas density. f_c is the fraction of the 2-photon continuum emitted by the HH object which is intercepted by the portion of flow cavity wall encompassed by the instrumental beam used to measure the [CII]158μm flux, and can be derived with simple geometrical considerations. The radius of the HH object is set to 5″ (see above).

A critical parameter in Eq.(2) is the factor η_{ce} which accounts for the collisional enhancement of the hydrogenic 2s level population above the values predicted by pure recombination. η_{ce} can be determined from a comparison of the predicted two-photon spectrum with the observed UV continuum from HH objects. Dopita, Binette & Schwartz (1982) find values $5.5 \leq \eta_{ce} \leq 10.6$ for the different knots of HH 1, and $2.8 \leq \eta_{ce} \leq 6.2$ for the different knots of HH 2. Since most of the knots in the two pointings will be encompassed by the LWS beam, we will adopt the mean η_{ce} values.

Another important parameter is the fraction χ_c of the incident FUV field which is re-radiated via the [CII]158μm line; this parameter is predicted to vary between 0.1% and 1% (Tielens & Hollenbach 1985). Since the rest of the FUV flux is reprocessed by dust into Far-IR continuum, our data should in principle allow us to independently estimate χ_c as the ratio between the [CII]158μm line flux and the integrated FIR continuum as revealed by the LWS. Indeed, LWS observations clearly reveal significant continuum emission

longward of $\sim$50μm toward all pointings. The full spectra are shown in Fig. 3, where the minispectra from the ten detectors have been stitched together for cosmetic purposes. The region is quite complex at these wavelengths and our continuum data do not represent an improvement, given the relatively poor spatial resolution, with respect to previous studies. Our data are in substantial agreement with Cohen et al. (1984), also considering that our pointed positions do not match the emission peaks of the bipolar emission pattern mapped at 100μm with the KAO. The peak wavelengths in the SEDs of Fig. 3 imply black-body dust temperatures of 25, 32 and 47 K toward HH 2, VLA 1 and HH 2 respectively, in agreement with the KAO observations of Harvey et al. (1986). The origin of the FIR continuum is not easy to assess. Cohen et al. (1984) do not detect 100μm emission from HH 2 to a 3σ limit of $\sim$12Jy; clearly, a portion of the continuum that we detect toward HH 2 is due to contamination from VLA 1. As concerns HH 1 it is clear form the KAO data that a significant portion of the FIR continuum comes from a radio source $\sim$30$''$ S-SW of HH 1 and associated with an H_2O maser (Pravdo et al. 1985). Based on the same dataset, it seems also clear that the C-S star does not seem to significantly contribute longward of 50μm; this is not surprising given its state of relatively evolved PMS star.

EDITOR: PLACE FIGURE 3 HERE.

The pointing where a more reliable estimate of the PDR FIR continuum can be derived is probably HH 2. Indeed, the HH 1 continuum is severely contaminated by two sources (see above), while the VLA 1 continuum is likely dominated by thermal dust emission in the envelope of this Class 0 source. HH 2 instead, may only partially be contaminated by the VLA 1 continuum. The [CII]158μm/FIR ratio toward HH 2 yields $\chi_c \geq 0.005$, clearly in the range of values expected from the PDR models.

With this choice of parameters we run our models (Molinari, Noriega-Crespo &

Spinoglio 2001) to determine the quantities in Eqs.(1) and (2) as a function of the gas density n (in cm^{-3}) and shock compression ratio $\mathcal{R}$=n/n_0. The resulting grids are presented in Fig. 4 (full-line for HH 2, dashed-line for HH 1). The figure also shows the location of the HH objects based on the 6 cm flux observed by Rodríguez et al. (1990), and the [CII]158μm observed with the LWS, decreased by an amount $\sim 3.5\ 10^{-19}$ W cm^{-2} which is our estimate of the maximum contribution due to external FUV irradiation (§4.1.1).

EDITOR: PLACE FIGURE 4 HERE.

The adopted model seems successful in reproducing the observable quantities. Formal values of density and compression ratio are [n, $\mathcal{R}$]=[(5200,5100), (40,18)] for HH 1 and 2 respectively. A problem with this scenario, however, is that we seem to produce too much FUV continuum. The predicted *emitted* flux at the indicative wavelength of 1500Å for the adopted model parameters is $\sim 8\,10^{-13}$ ergs s^{-1} cm^{-2} $Å^{-1}$, which should be compared with the dereddened observed values of $\sim 10^{-13}$ ergs s^{-1} cm^{-2} $Å^{-1}$ for the two HH objects (e.g., Böhm-Vitense et al. 1982). We can tune the model parameters to produce less FUV continuum and still fit the [CII]158μm and 6 cm observations. For example, we may decrease the radii of the ionized regions by 50%, which is not unreasonable since we estimated this parameter directly from plots of radio maps. Additionally, we can also increase χ_c; in low irradiation conditions, like in the present case, this parameter can reach values ~ 0.01 (Tielens & Hollenbach 1985) which is not in contradiction with our previous estimate as this was a lower limit due to the difficulty of assessing the intrinsic FIR continuum of the HH objects (see above). With this choice of parameters we still fit the observed [CII]158μm line flux and 6 cm radio continuum, but with densities a factor 2 higher and compression ratios a factor 2 lower, producing an emitted 1500Å continuum of $\sim 3\,10^{-13}$ ergs s^{-1} cm^{-2} $Å^{-1}$; the discrepancy with UV observations is reduced to a factor 3, which could be partly accounted for by the uncertainties in the reddenening corrections applied.

As concerns the jet emanating from VLA 1, its low ionization (Solf & Böhm 1991) also confirmed by the low radio flux measured (e.g., Rodríguez et al. 1990) is not sufficient to produce the amount of FUV continuum that would be required by our models to induce the [CII]158μm emission observed toward VLA 1. In the absence of significant dust column along the line of sight from the HH objects to the proximity of VLA 1, however, the direct FUV irradiation from the HH objects onto the cavity walls at the base of the flow would be sufficient to justify the [CII]158μm line flux observed toward VLA 1. The observation of a scattered-light component in the [SII]$\lambda\lambda$6716,6731 line along the jet (Solf & Böhm 1991), and the presence of a biconical nebula seen in scattered optical light at the base of the jet (Strom et al. 1985) would indeed seem to strengthen the idea of a relatively dust-free flow cavity (see also Davis, Eislöffel & Ray 1994).

4.1.3. Line cooling

We are now able to estimate the amount of cooling expected in lines other than [CII]158μm in the PDR conditions discussed above. The external and relatively faint FUV field ($G_0 \sim 7$) from the Orion Nebula can generate F([OI]63μm)$\sim$5%F([CII]158μm), at most, for n$\sim 10^3$ cm^{-3}. Increasing the density will also increase the expected [OI]63μm/[CII]158μm cooling ratio (Kaufman et al. 1999), but the absolute [CII]158μm flux emitted would also decrease by a similar amount living the absolute [OI]63μm cooling essentially unaltered. As concerns the local FUV field, the G_0 value for the PDR will be dependent on the assumed distance between the HH objects and the flow cavity walls. The CO maps of Moro-Martín et al. (1999) reveal a full width of the low-velocity lobes in the HH 1/2 outflow of the order of $\sim 30''$, implying $G_0 \sim 40$ at the cavity walls and a maximum [OI]63μm PDR cooling $\sim 20 \div 30$% of the [CII]158μm. As noted above, the *absolute* [OI] cooling is almost independent on the assumed density.

Finally, high-J CO and rotational H_2 lines fluxes comparable to the observed values can only be generated in energetic ($G_0 \geq 10^3$) and very dense (n$\geq 10^6$ cm^{-3}) PDRs (e.g., Burton, Hollenbach & Tielens 1990, which is clearly not the present case.

4.2. Shock conditions in the HH objects

4.2.1. Atomic lines

The shock conditions toward HH 1 and 2 were diagnosed comparing our observations (after correcting the [OI] lines for PDR contamination, see §4.1.3) with the predictions from plane parallel atomic shock models. The shock models were calculated using MAPPINGS2, a code developed by Binette, Dopita & Tuohy (1985), which has been thoroughly tested (Pequignot 1986). A grid of models was created changing the pre-shock density between 10^2 and 10^4 cm^{-3}, and the shock velocity between 60 and 140 km s^{-1}. The rest of the model parameters have been fixed to standard values (Molinari, Noriega-Crespo & Spinoglio 2001). The [OI]63μm/[OI]145μm−[NeII]12.8μm/[SiII]34.8μm diagram in Fig. 5 shows that shock velocities of v_s ∼100 or ∼140 km s^{-1}, and pre-shock densities between 10^2 and 10^3cm^{-3} would be adequate to describe the observed line ratios. Higher shock velocities seem to be ruled out since [NeII]12.8μm/[SiII]34.8μm ratios largely in excess with respect to the observations are produced (e.g., ∼10 for v_s ∼220 km s^{-1}, using the planar shock models of Hartigan, Raymond & Hartmann (1987)). We note that the beamsize of the SWS at the [SiII]34.8μm wavelength is a factor ∼ 1.7 larger than at the [NeII]12.8μm wavelength, but this would not change the position of the HH objects in Fig. 5 by a significative amount even for uniformly extended emission. Noticeably, the estimated pre-shock densities are in good agreement with the independent estimates based on the shock-excited PDR model (§4.1.2). Those models were computed using v_s=100 km s^{-1}, but we note that the adoption of v_s=140 km s^{-1} would simply imply, according to Eq. (1), a right-shift of the model grids

in Fig. 4, still fitting the observations (with higher compression ratios, though).

EDITOR: PLACE FIGURE 5 HERE.

The comparison with optical line diagnostics is not straightforward given the complex morphology of the HH objects which appear structured in several knots, both in optical and near-IR images, which our observations do not spatially resolve (Herbig & Jones 1981; Noriega-Crespo & Garnavich 1994; Davis, Eislöffel & Ray 1994). The SWS pointing toward HH 1 encompasses knots A, C, D and F; optical lines suggest shock velocities $\sim 80 \mathrm{km\,s^{-1}}$ for A, and consistently above $130 \mathrm{km\,s^{-1}}$ for all the others (Hartigan, Raymond & Hartmann 1987). The dust scattered emission requires at least 150 $\mathrm{km\,s^{-1}}$ shocks to explain the optical observations (Noriega-Crespo, Calvet & Böhm 1991). Our estimate of $v_s \sim 100 \mathrm{km\,s^{-1}}$ might represent average physical conditions over the SWS beamsize, although the negative detection of [OIII]88μm in the present observations (expected to be at the same flux level of the [OI]63μm line) cannot in principle be explained with $v_s \geq 130 \mathrm{km\,s^{-1}}$. The presence of strong [O III] 4959+5007 Å, however, in HH 1F and HH 2A+H (Solf & Böhm 1991) sets a lower limit at ~ 100 $\mathrm{km\,s^{-1}}$ for the shock velocity and suggests that other mechanisms like, e.g., partial ionization of the pre-shock material, may be responsible for the depression of [OIII]88μm flux levels. Likewise, the SWS pointing toward HH 2 includes knots A, B, C, G, H and M, where shock velocities estimated from optical lines range from 100 to 200 $\mathrm{km\,s^{-1}}$ (Hartigan, Raymond & Hartmann 1987; Solf & Böhm 1991).

4.2.2. Molecular lines

Pure rotational H_2 lines in the ground vibrational level are normally analyzed under LTE conditions (e.g., Gredel 1994). Einstein coefficients and wavenumbers were taken from Black & Dalgarno (1976) and Dabrowski (1984), and an ortho/para=3 has been

assumed. The SWS aperture at the S(1) and S(2) line wavelengths is a factor ~ 1.7 larger compared with the other H_2 lines; fluxes for these two lines were corrected accordingly, assuming extended and uniform emission. We dereddened the H_2 line fluxes using the visual extinctions given by Böhm et al. (1987) and using the Rieke & Lebofsky (1985) extinction curve. The H_2 gas temperature and column density can then be directly obtained from the slope and intercept of a linear fit to the Boltzmann plots shown in Fig. 6, and are reported in Table 2 together with 1σ uncertainties in parenthesis; a solid angle equal to the SWS focal plane aperture for the S(3)-S(5) lines was assumed, i.e. $14''$ x $20''$ or 6.6×10^{-9} sr (valid for all detected H_2 lines but S(1), where the solid angle is $\sim$30% higher), with a beam filling factor of 1. The fits show that a single temperature component is adequate to represent the observations, given the observational uncertainties.

EDITOR: PLACE FIGURE 6 HERE.

Using the same model and the parameters determined from the Boltzmann plots, we can estimate an H_2 cooling, for the component traced by the (0-0) lines, of 9 10^{-3} $L_\odot$ and 2.5 10^{-2} $L_\odot$ for HH 1 and HH 2, respectively.

EDITOR: PLACE TABLE 2 HERE.

The issue of the nature of the H_2 excitation in HH 1 and 2 has been discussed by several authors in the last decade using near-IR imaging of the S(1)1-0 2.12μm and near-IR spectra in the H and K bands (Noriega-Crespo & Garnavich 1994; Davis, Eislöffel & Ray 1994; Gredel 1996; Eislöffel, Smith & Davis 1996; Davis, Smith & Eislöffel 2000). The spectra suggest excitation temperatures ranging between 2000 and 3000 K in the various emission knots revealed in the images. Detailed modeling suggests that C-type (Draine 1980) shocks best fit the observational scenario; H_2 emission would originate in the tails

of the bow-shocks, whose tips are instead bright in [FeII]1.64μm (Davis, Eislöffel & Ray 1994), where the shock velocities are low enough for H_2 not to be dissociated. The fact that Boltzmann plots based on H_2 ro-vibrational are satisfactorily fitted with single linear fits led Gredel (1996) to doubt as to the C shock origin, since a stratification of temperatures up to ~ 3000 K should be expected. Eislöffel, Smith & Davis (1996) review the most popular shock models and indeed confirm that curved C-type shocks produce a quite shallow trend in the Boltzmann plots; besides, the predicted excitation temperatures of the $v = 1$ lines are significantly lower (~ 1000 K) than actually observed. Planar C-type shocks, on the other hand, seem to produce a rather abrupt change of slope at upper energy levels $\sim 4000 - 5000$ K. Since this is exactly at the separation between the $v = 0$ lines we detected in the present work and the $v > 0$ lines detected in the near-IR, the combined analysis of mid- and near-IR H_2 lines seems to suggest an origin in planar C-type shocks.

C-type shocks are good emitters of molecular lines in general. Our marginal detection of high-J CO lines at flux levels comparable to H_2 (0-0) lines suggests shock velocities $15 \leq v_s \leq 20$ km s^{-1} and pre-shock densities $n_0 \geq 10^5$ cm^{-3} (Kaufman & Neufeld 1996). However, for the same parameters the model also predict an $H_2O(2_{12}$-$1_{01})$ line flux about two orders of magnitude higher than actually observed in HH 2 (Tab. 1). Unless H_2O vapor is confined in a much smaller area compared to H_2 or CO, there is a clear deficit with respect to expectations. This seems unusual for Class-0 objects (Giannini, Nisini & Lorenzetti 2001) and resembles more evolved Class-I systems. The possibility that water vapor depletes onto grains in the post-shock cooling region has been verified for HH 7 in NGC 1333 with the detection of the 62μm ice band (Molinari et al. 1999); we do not detect such a feature anywhere in the HH 1/2 system, although the filling factor of the bow-shocks present in HH 1 and 2 (e.g., Fig. 1) in the LWS beam is lower than in the case of HH 7 (also because of the larger distance). An interesting alternative to explain the water vapor deficit could be offered by the marginal detection of the fundamental lines of the OH molecule in

HH 2. Given the high velocity of the dissociative shocks in HH 1/2, significant amounts of Far-UV flux can be expected to be irradiated by the post-shock regions (see § 4.1); in particular, the photons between 1300Å and 2000Å are capable of dissociating the water molecule into H and OH (Andresen, Thissen & Schroeder 2001). Water photodissociation by a UV field was also invoked by Spinoglio et al. (2000) to explain the surprisingly high OH cooling found toward T Tau.

Comparing the v_s ∼20 km s^{-1} found for the C-type molecular shocks with the v_s ∼100 km s^{-1} deduced for the dissociative J-type shock traced by the atomic lines (§ 4.2.1), it is plausible that the two shock regions are respectively associated with the tails and tips of bow-shocks. Such structures are indeed identified in HH 1 and, with a more complex morphology, in HH 2 (Hester, Stapelfeldt & Scowen 1998). The 2 orders of magnitude difference in pre-shock densities implies that significant compression of the pre-shock material has taken place in the molecular shocks. This is expected given the very nature of the C-type shocks, where the relatively low shock velocity and the presence of transverse magnetic field combine to accelerate and pre-compress the upstream material. I-band polarimetry (Strom et al. 1985) indeed confirms the presence of a magnetic field oriented along the HH 1/2 flow.

S.M. thanks the generous support of NASA Jet Propulsion Laboratory through contract 1227169. A.N-C. research has been supported in part by NASA ADP grant NRA-00-01-ADP-096. The paper's clarity considerably improved thanks to the comments of an anonymous referee. ISAP is a joint development by the LWS and SWS Instrument Teams and Data Centers. Contributing institutes are CESR, IAS, IPAC, MPE, RAL and SRON. LIA is a joint development of the LWS consortium. Contributing institutes are RAL, IPAC and CESR. OSIA is a joint development of the SWS consortium. Contributing institutes are SRON, MPE and KUL.

REFERENCES

Andresen, P., Thissen, T., Schroeder, K. 2001, ApJ, 550, 346

Binette, L., Dopita, M.A., & Tuohy, I.R. 1985, ApJ, 297, 476

Black, J.H., Dalgarno, A. 1976, ApJ, 203, 132

Böhm, K.H., Bührke, Th., Raga, A.C., Brugel, E.W., Witt, A.N., Mundt, R. 1987, ApJ, 316, 349

Böhm, K.H., Noriega-Crespo, A., Solf, J. 1993, ApJ, 416, 647

Böhm-Vitense, E., Böhm, K.H., Cardelli, J.A., Nemec, J.M. 1982, ApJ, 262, 224

Burton, M.G., Hollenbach, D.J., Tielens, A.G.G.M. 1990, ApJ, 365, 620

Cernicharo, J., Cesarsky, D., Noriega-Crespo, A., Lefloch, B. & Moro-Martín, A. 1999 in "H_2 in Space" F. Combes & G. Pineau des Forêts, Cambridge University Press, 23

Clegg, P.E., Ade, P.A.R., Armand, C., et al. 1996, A&A, 315, L38

Cohen, M., Schwartz, R.D. 1979, ApJ, 233, L77

Cohen, M., Harvey, P.M., Schwartz, R.D., Wilking, B.A. 1984, ApJ, 278, 671

Curiel, S., Cantó, J., Rodríguez, L.F. 1987, Rev. Mexicana Astron. Af., 14, 595

Dabrowski, I. 1984, Can. J. Phys., 62, 1639

Davis, C.J., Eislöffel, J., Ray, T.P. 1994, ApJ, 426, L93

Davis, C.J., Smith, M.D., Eislöffel, J. 2000, MNRAS, 318, 747

de Graauw, Th., Haser, L.N., Beintema, D.A., et al. 1996, A&A, 315, L49

Dopita, M.A., Binette, L., Schwartz, R.D. 1982, ApJ, 261, 183

Draine, B.T. 1980, ApJ, 241, 1021

Eislöffel, J., Mundt, R., & Böhm, K.-H. 1994, AJ, 108, 1042

Eislöffel, J., Smith, M.D., Davis, C.J. 2000, A&A, 359, 1147

Giannini, T., Nisini, B., Lorenzetti, D. 2001, ApJ, 555, 40

Gredel, R. 1994, A&A, 292, 580

Gredel, R. 1996, A&A, 305, 582

Habing, H.J. 1968, Bull. Astr. Inst. Netherlands, 19, 421

Hartigan, P., Raymond, J., Hartmann, L. 1987, ApJ, 316, 323

Hartigan, P., Morse, J., Raymond, J. 1994, ApJ, 436, 125

Harvey, P.M., Joy, M., Lester, D.F., Wilking, B.A. 1986, ApJ, 301, 346

Herbig, G.H., & Jones, B.F. 1981, AJ, 86, 1232

Hester, J.J., Stapelfeldt, K.R., Scowen, P.A. 1998, AJ, 116, 372

Hollenbach, D.J., McKee, C. 1989, ApJ

Kaufman, M.J., Neufeld, D.A. 1996, ApJ, 456, 611

Kaufman, M.J., Wolfire, M.G., Hollenbach, D.J., Luhman, M.L. 1999, ApJ, 527, 795

Kessler, M.F., Steinz, J.A., Anderegg, M.E., et al. 1996, A&A, 315, L27

Molinari, S., Ceccarelli, C., White, G.J., et al. 1999, ApJ, 521, L71

Molinari, S., Noriega-Crespo, A., Ceccarelli, C. et al. 2000, ApJ, 538, 698

Molinari, S., Noriega-Crespo, A., Spinoglio, L. 2001, ApJ, 547, 292

Moro-Martín, A., Cernicharo, J., Noriega-Crespo, A., & Martín-Pintado, J. 1999, ApJ, 520, L111

Mundt, R., Witt, A.N. 1983, ApJ, 270, L59

Noriega-Crespo, A. Calvet, N., Böhm, K.H. 1991, ApJ, 379, 676

Noriega-Crespo, A., Garnavich, P. 1994, AJ, 108, 1432

Noriega-Crespo, A., Garnavich, P., Curiel, S., Raga, A.C., & Ayala, S. 1997, ApJ, 486, 55

Ogura, K. 1995, ApJ, 450, L23

Pequignot, D. 1986 in "Workshop on Model Nebula", Observatoire de Paris, D. Péquignot ed. p. 363

Pravdo, S.H., Rodríguez, L.F., Curiel, S. et al. 1985, ApJ, 293, L35

Raga, A.C. 1994, Ap&SS, 216, 105

Rieke, G.H., Lebofsky, M.J. 1985, ApJ, 288, 618

Reipurth, B. 1999 in http://casa.colorado.edu/hhcat/

Rodríguez, L.F., Ho, P.T.P., Torrelles, J.M., Curiel, S., Cantò, J. 1990, ApJ, 352, 645

Rodríguez, L.F., Delgado-Arellano, V.G., Goméz, Y. et al. 2000, AJ, 119, 882

Saraceno, P., Nisini, B., Benedettini, M. et al. 1998 in "Star Formation with the Infrared Space Observatory" Joao Yun & Rene Liseau eds., ASP, 132, 233

Solf, J. ,Böhm, K.-H. 1991 ,ApJ, 375, 618

Solf, J. ,Böhm, K.-H., Raga, A. 1988 ,ApJ, 334, 229

Spinoglio, L., Giannini, T., Nisini, B., et al. 2000, A&A, 353, 1055

Strom, S.E., Strom, K.M., Grasdalen, G.L., et al. 1985, AJ, 90, 2281

Tielens, A.G.G.M., Hollenbach, D. 1985, ApJ, 291, 722

Fig. 1.— HST [SII] image of the HH 1/2 region. The crosses mark the pointed positions, while dashed circles and full-line rectangles indicate the FWHM beamsizes of the LWS and SWS respectively. The position of the C-S star is also indicated.

Fig. 2.— **a.** H_2, [NeII]12.8μm and [SiII]34.8μm lines detected toward HH 1 (left column) and HH 2 (right column).

Fig. 2.— **b.** [OI]63μm lines detected toward the three positions observed with the LWS.

Fig. 2.— **c.** Lines detected between 110 and 180μm toward the three positions observed with the LWS.

Fig. 3.— Spectral energy distributions observed with LWS toward all pointings. The 10 LWS detectors have been stitched together to produce a smooth SED. No correction has been applied for the reciprocal contamination between adjacent beams.

Fig. 4.— [CII]158μm line flux as a function of 6 cm radio continuum flux expected for PDR emission induced by the FUV two-photon continuum from the ionized regions in the HH objects. The grids show the loci of points of constant density n (horizontal lines) and constant $\mathcal{R}$=n/n$_0$ compression ratio in case of a recombination region 5″ in radius behind a shock front in a HH object with v$_s$=100 km s^{-1}. The other parameters used are [η_{ce}, χ_c]=[(8.0,4.5),(0.005,0.005)] for the dashed and full-line grids (HH 1 and HH 2) respectively.

Fig. 5.— Diagnostic diagram showing the model results for the indicate line ratios; full lines are the loci of constant shock velocity (from 60 to 136 km s^{-1}), while dashed lines are loci of constant pre-shock density (from 10^2 to 10^4 cm^{-3}).

Fig. 6.— H_2 excitation diagrams (Boltzmann plots) for HH 1 and HH 2 (empty and full circles respectively). N_j/g_j is reported as a function of the energy of the level in K. The full lines represent linear regressions to the data points.

Table 1. Observed Line Fluxes

Line	$\lambda(\mu$m)	VLA 1	HH 1	HH 2
		SWS Lines		
(0-0)S(1)	17.03	···	0.7(0.3)	2.8(0.3)
(0-0)S(2)	12.28	···	2.3(0.5)	3.1(0.3)
(0-0)S(3)	9.66	···	3.0(0.6)	5.8(0.9)
(0-0)S(4)	8.03	···	1.8(0.8)	4.7(0.5)
(0-0)S(5)	6.91	···	3.6(0.9)	14(2)
[NeII]	12.81	···	4.7(0.9)	6.8(0.7)
[SiII]	34.82	···	5(1)	6(1)
		LWS Lines		
CO 18-17	144.8	2(1)		
CO 17-16	153.3			3.0(0.6)
CO 16-15	162.8	6.8(0.7)	5(2)	4(2)
		(5.7)	*(4)*	*(3)*
OH[3/2,5/2-3/2,3/2]	119.3			4(1)
OH[3/2,1/2-1/2,1/2]	163.2			3(2)
o-$H_2O[2_{12}$-$1_{01}]$	179.5			7(2)
[OI]	63.18	173(2)	101(2)	150(3)
		(151)	*(86)*	*(135)*
[OI]	145.5	5(1)	4(1)	4(1)
		(4)	*(4)*	*(4)*
[CII]	157.7	79(1)	90(3)	82(3)
		(63)	*(84)*	*(76)*

Table 2. H_2 Physical Parameters

Object	T_{H_2} (K)	$N(H_2)$ (10^{19} cm^{-2})
HH 1	670(40)	1.1(0.4)
HH 2	730(20)	2.2(0.3)

Note. — Based on aperture-corrected line fluxes (see text).

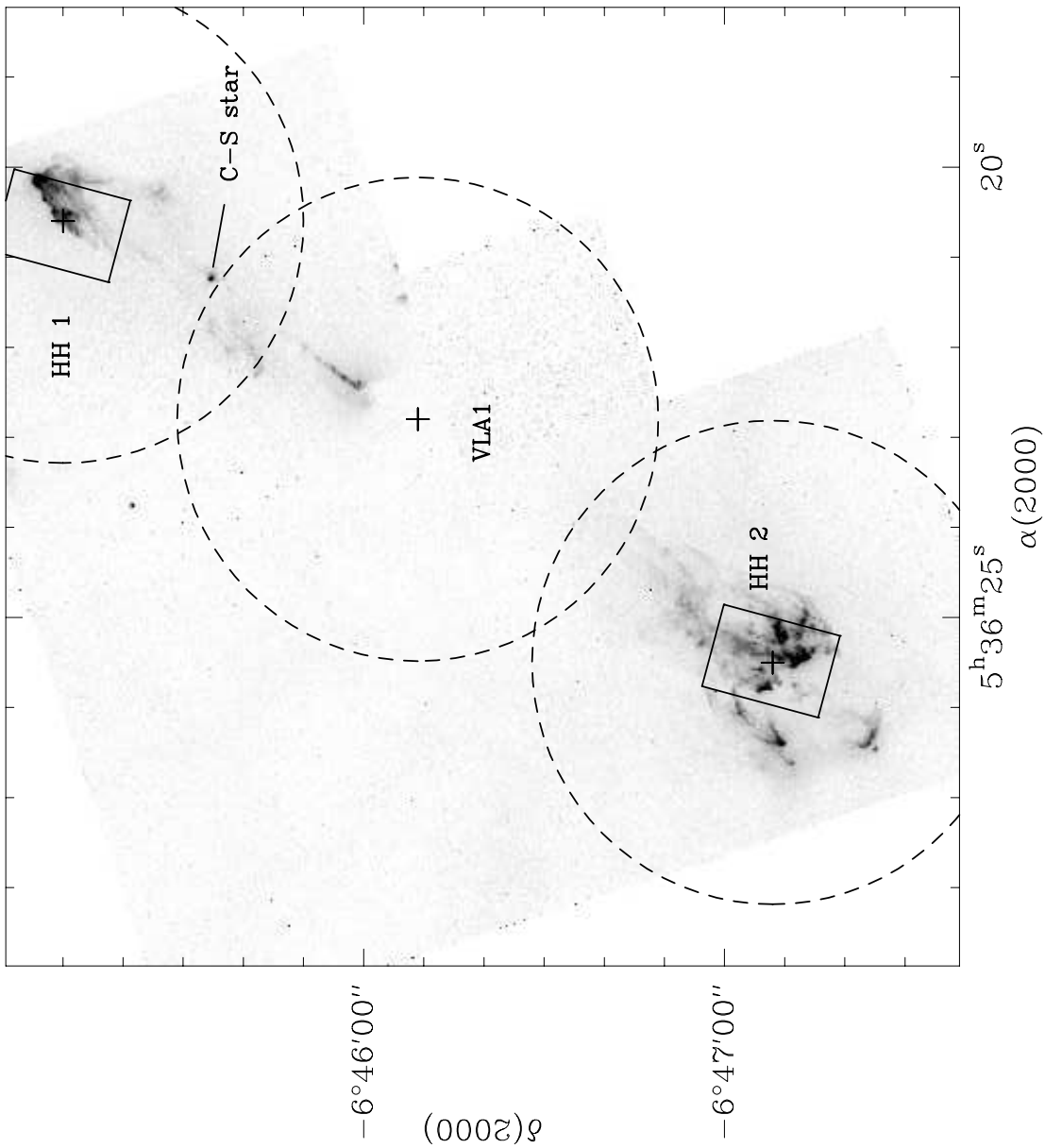
HH 1
C–S star
VLA1
HH 2
−6°46′00″
−6°47′00″
δ(2000)
5h36m25s
20s
α(2000)

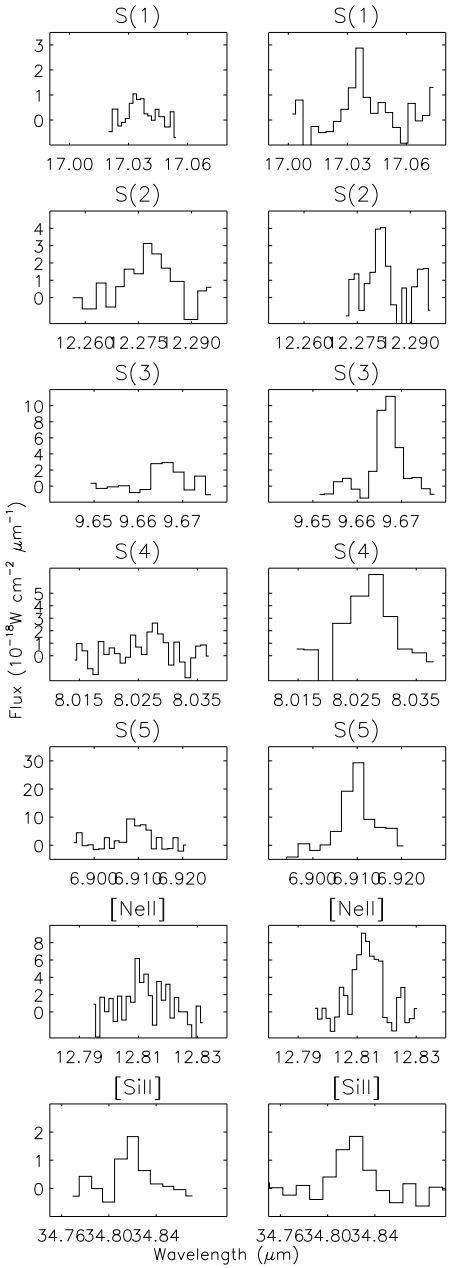
S(1)
S(1)
S(2)
S(2)
S(3)
S(3)
S(4)
S(4)
S(5)
S(5)
[NeII]
[NeII]
[SiII]
[SiII]
Flux (10^{-18}W cm^{-2} μm^{-1})
Wavelength (μm)

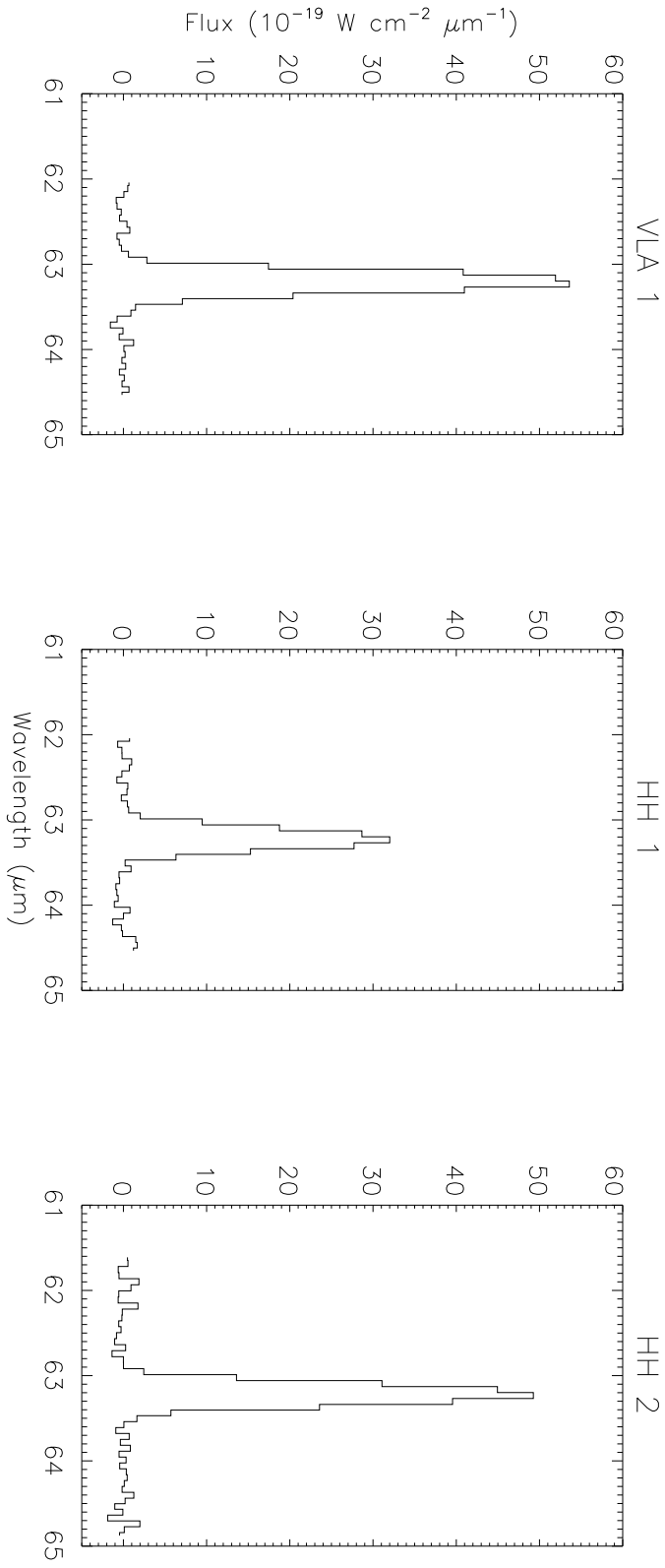
Flux (10^{-19} W cm^{-2} μm^{-1})
VLA 1
HH 1
HH 2
Wavelength (μm)
0
10
20
30
40
50
60
61
62
63
64
65

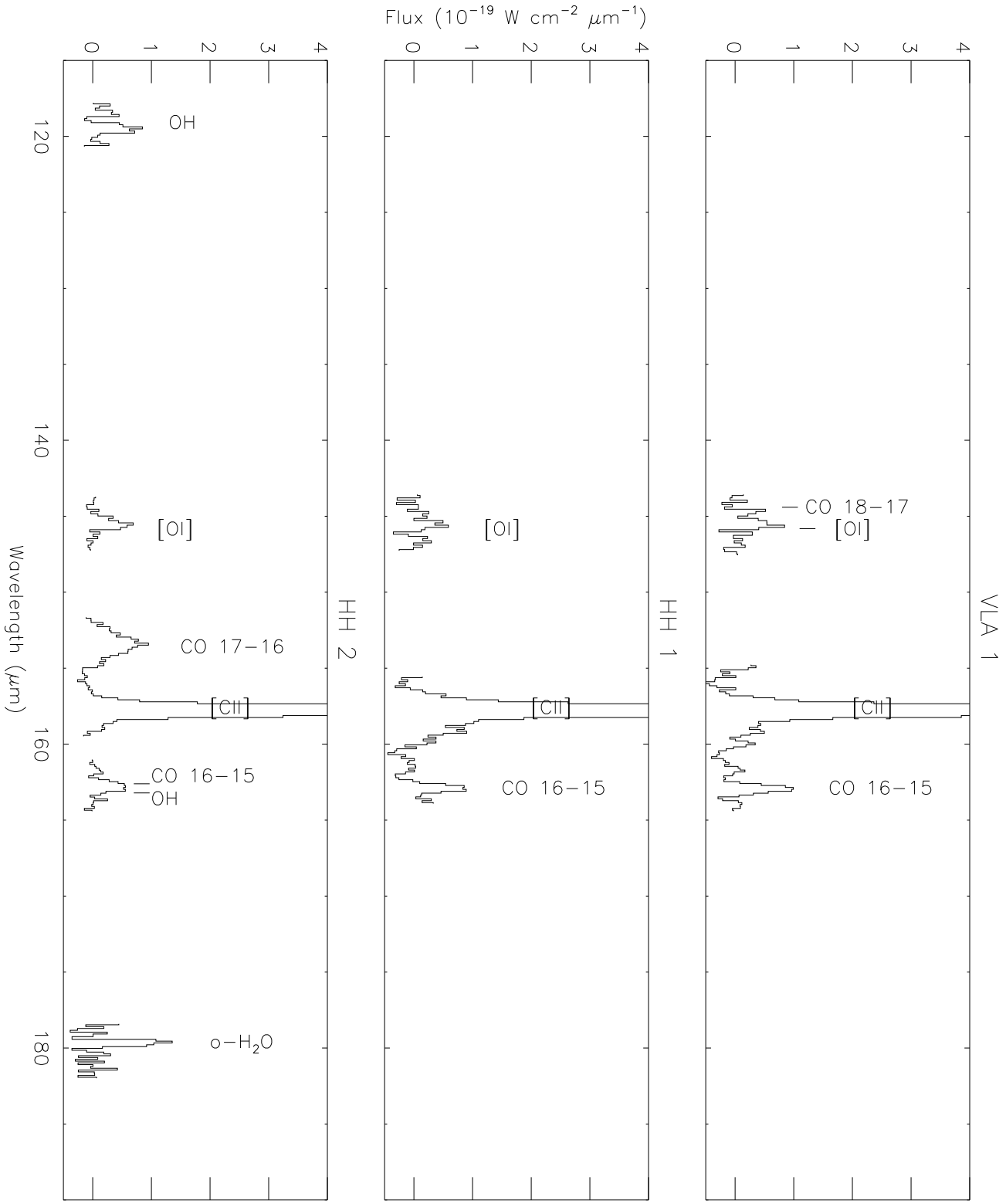
Flux (10^{-19} W cm^{-2} μm^{-1})
0
1
2
3
4
Wavelength (μm)
120
140
160
180
OH
[OI]
CO 17–16
[CII]
CO 16–15
OH
o–H$_2$O
HH 2
HH 1
VLA 1
CO 18–17
[OI]
[CII]
CO 16–15

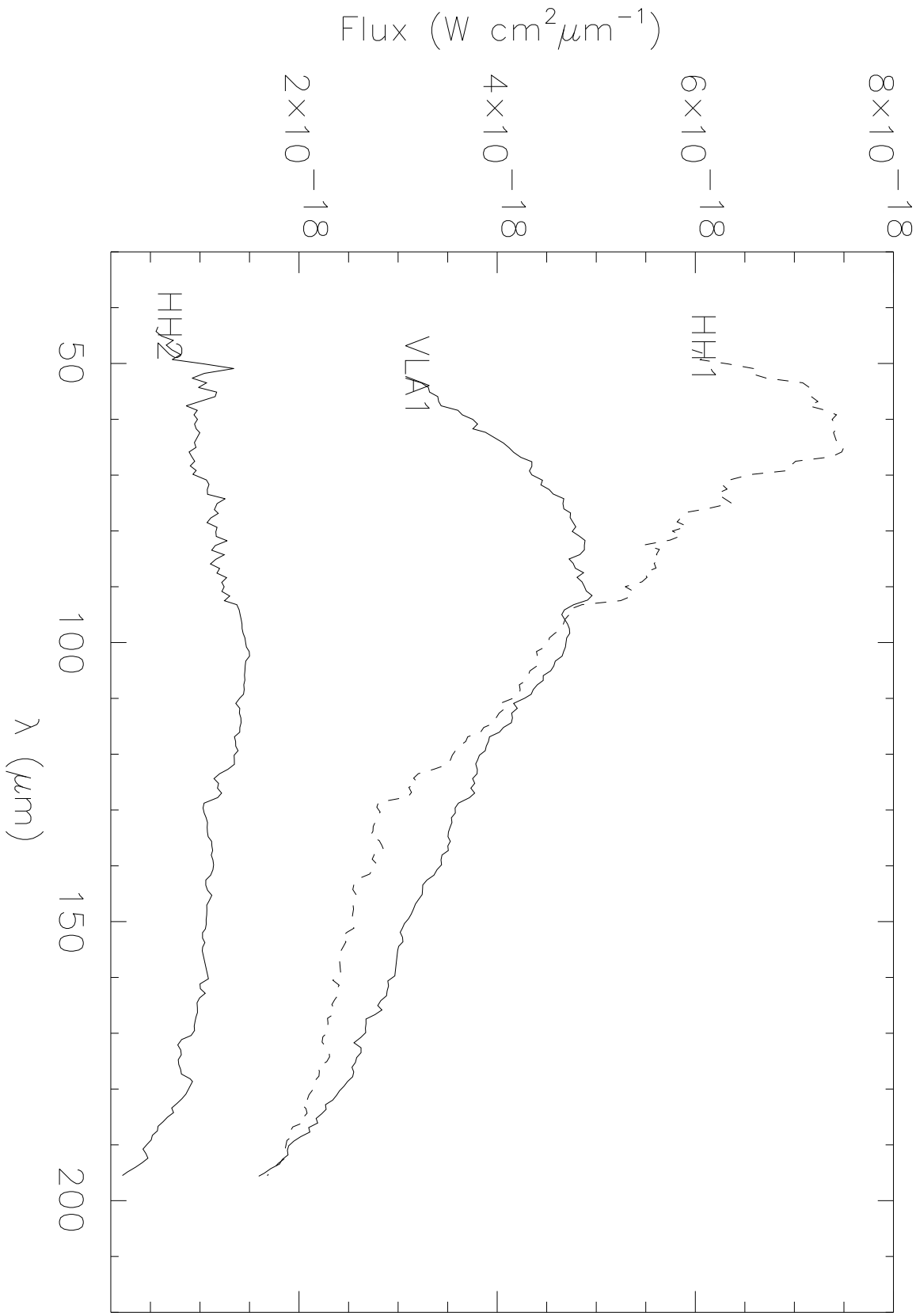
Flux (W cm^2 μm^{-1})
2×10−18
4×10−18
6×10−18
8×10−18
HH2
VLA1
HH1
50
100
150
200
λ (μm)

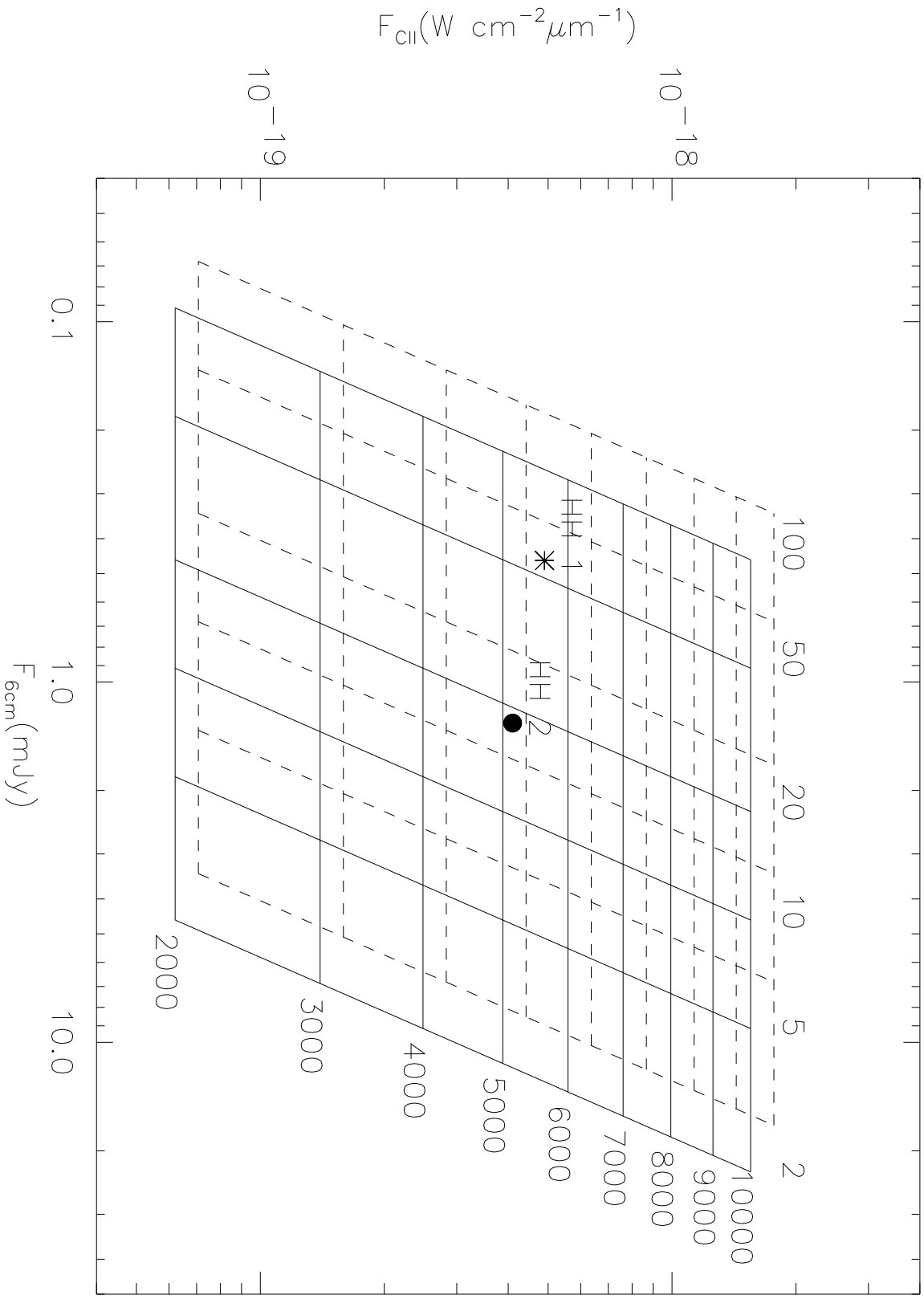
F_{CII}(W cm$^{-2}\mu$m^{-1})
10^{-19}
10^{-18}
100
50
20
10
5
2
HH 1
HH 2
0.1
1.0
10.0
F_{6cm}(mJy)
2000
3000
4000
5000
6000
7000
8000
9000
10000

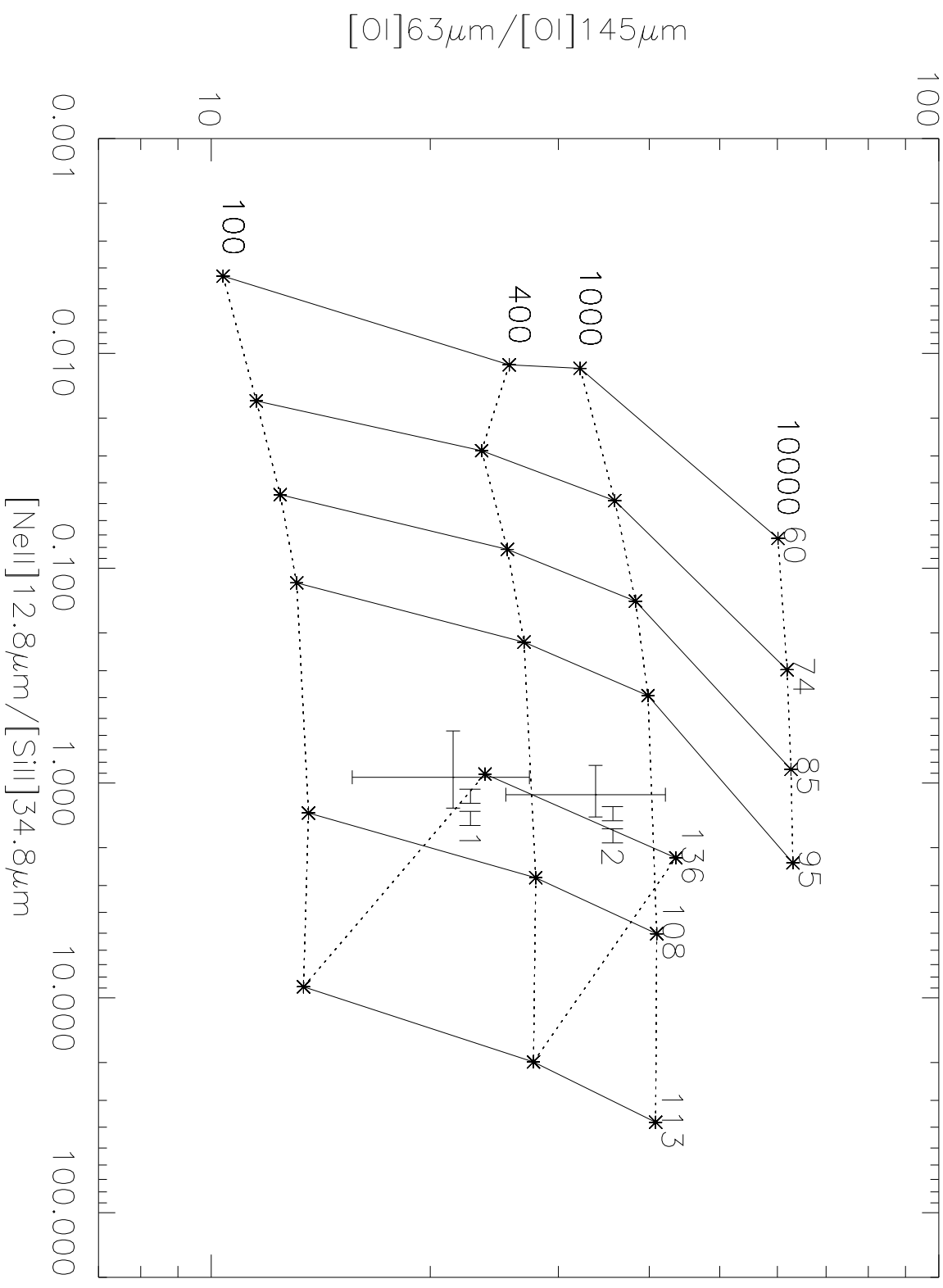
[OI]63μm/[OI]145μm
100
10
0.001
0.010
0.100
1.000
10.000
100.000
[NeII]12.8μm/[SiII]34.8μm
100
400
1000
10000
60
74
85
95
136
108
113
HH1
HH2

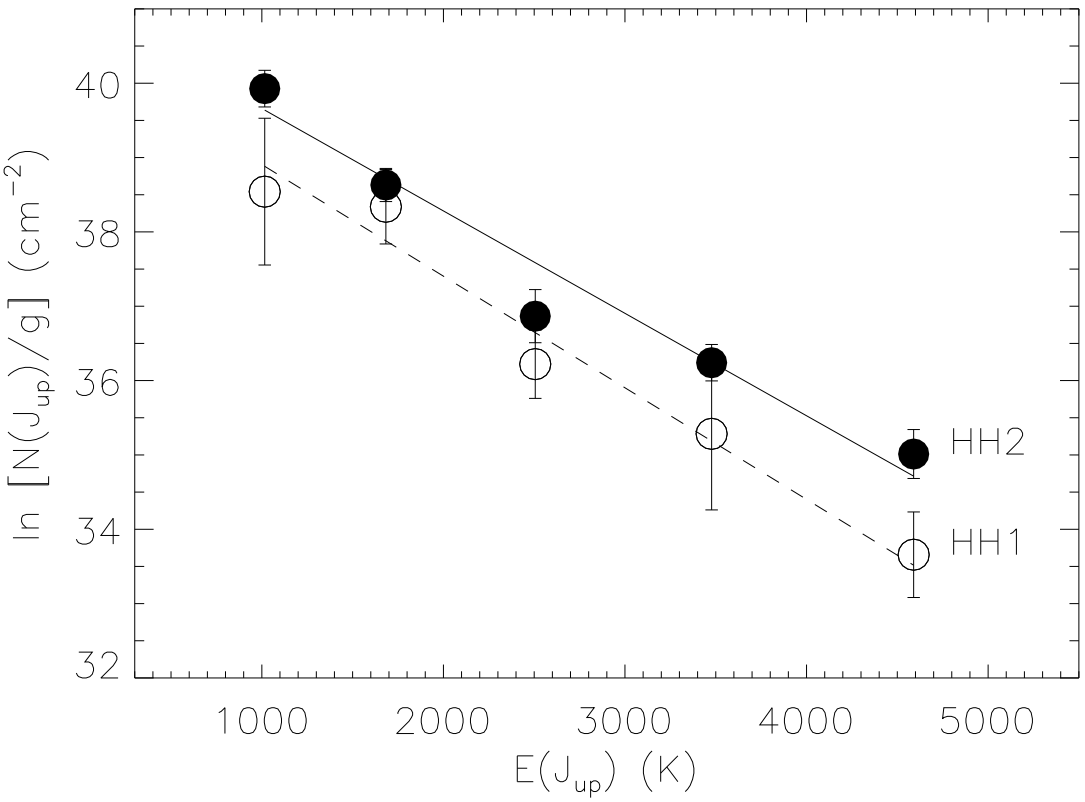
40
38
36
34
32
1000
2000
3000
4000
5000
ln [N(J_up)/g] (cm^-2)
E(J_up) (K)
HH2
HH1